Modeling and Control of Soft Robotic Tail Based Aerial Maneuvering (STAM) System: Towards Agile Self-Righting with a Soft Tail

Conference Paper · October 2021

DOI: 10.1109/ICAR53236.2021.9659375

6 authors, including:

Jawad Mehmood Butt
The Chinese University of Hong Kong
4 PUBLICATIONS **9** CITATIONS
SEE PROFILE

Xiangyu Chu
The Chinese University of Hong Kong
15 PUBLICATIONS **21** CITATIONS
SEE PROFILE

Xiaomei Wang
The University of Hong Kong
11 PUBLICATIONS **102** CITATIONS
SEE PROFILE

Ka-Wai Kwok
The University of Hong Kong
120 PUBLICATIONS **1,682** CITATIONS
SEE PROFILE

2021 20th International Conference on Advanced Robotics (ICAR)
December 6-10, 2021. Ljubljana, Slovenia

Modeling and Control of Soft Robotic Tail Based Aerial Maneuvering (STAM) System: Towards Agile Self-Righting with a Soft Tail

Jawad Mehmood Butt*[1], Xiangyu Chu[1], Hao Zheng[1], Xiaomei Wang[2], Ka-Wai Kwok[2], and K.W. Samuel Au[1]

***Abstract*— Recent studies have demonstrated feasible aerial maneuvering with rigid tails. However, soft robotic tails were never investigated for aerial maneuvering applications, and no modeling strategy was found that exploits the soft robotic tail based aerial maneuvering (STAM) system kinematics for flight phase control (aerial self-righting). In this work, we provide the feasible solution to flight phase control of STAM systems (1-DOF and 2-DOF) by proposing their forward kinematics, differential kinematics, and flight phase models. We integrate Piecewise constant curvature (PCC) and Augmented rigid robot (ARR) modeling formulations to model the kinematics of 1-DOF STAM (body-tail pitch or body-tail yaw) system and propose its flight phase model & control. Then, we introduce the soft-tail "arbitrary-plane" bending which aids the extension of integrated modeling approaches to model the forward kinematics of 2-DOF (pitch and yaw) soft tail. The 2-DOF STAM system (body-tail pitch and yaw together) is composed of rigid body, cable-driven soft tail, and actuation units, so we develop their differential kinematics which maps the tail shape velocities with the body orientation angular rates and the tail cable velocities respectively. Together with the forward and differential kinematics, we present flight phase model and control of 2-DOF STAM system which ensures the conservation of total angular momentum. The simulations, which demonstrates the self-righting maneuvers with STAM systems are provided and the effective simulation results validates our proposed models.**

I. INTRODUCTION

Despite recent advances in robotic agile locomotion [1], [2], terrestrial robots capable of producing agile maneuvers in the air still lag far behind their biological counterparts [3]. Inspired by the dynamic capability of animal tails, researchers have developed various tail-inspired robots that were capable to generate agile maneuvers in the air. Initially, some simple 1-DOF tailed robots have been purposely developed to offer aerial maneuvers such as self-righting, self-stabilization, landing, and flipping [4]–[7], however, these maneuvers were only restricted to the plane. This restriction was tackled by the development of 2-DOF mechanically robust tailed-robots [8], [9] that were able to achieve the spatial maneuvers with appropriate controllers design [10]–[12]. These rigid-tail-based robots have successfully achieved the aerial maneuvering objective i.e., flight phase orientation control relying on the rigid-tail mechanisms. However, they still lag the natural maneuvering agility due to the rigid robotic tail stiffness and structural dissimilarity as compared to the animal tails [13]. To realize the bio-inspired dexterity and flexibility of robotic tails, a fish inspired soft robotic tail [14], continuum robotic tails (CRT) [15] [16] and articulated robotic tails (ART) were proposed [17]–[20]. Despite success of these tails in swimming [14], static stabilization, and spatial loading [13], [18], [20] research investigations, only few flexible tails were dynamically modeled [21] and empirically evaluated [16] to leverage their abilities for inertial application i.e., quadruped steering. However, soft robotic tails (SRT) were never used to explore the aerial maneuvering application, and no modeling strategy was found that exploits the STAM system (Fig. 1) kinematics behavior for flight phase control (conservation of total angular momentum) or aerial self-righting. Hence, there needs a simple and systematic kinematics based flight phase modeling approach which can guide the flight phase controller design process for complex locomotion task such

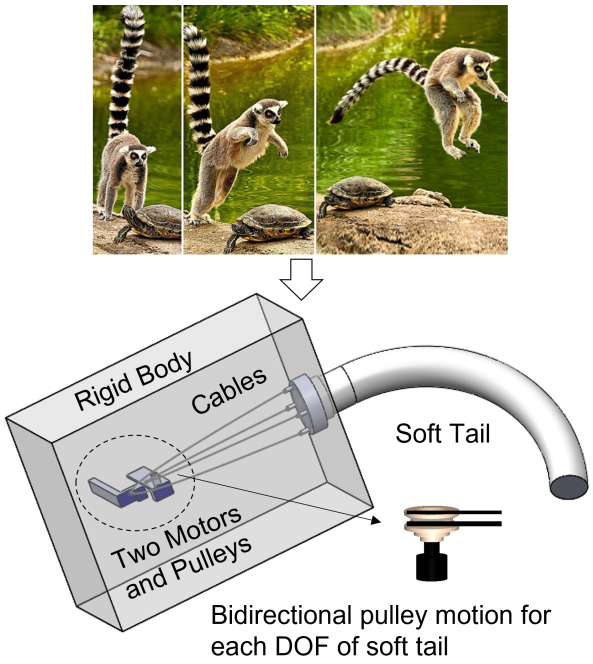

Fig. 1: Overview of our STAM system where the rigid body, soft tail and actuation system presents the animal trunk, tail and actuation joints respectively.

This work is supported by CUHK Chow Yuk Ho Technology Centreof Innovative Medicine, MRC, InnoHK, RGC GRF Ref No. 14209719,14209118, RGC T42-409/18-R, and Natural Science Foundation of China, U1613202.

The authors are with [1]Department of Mechanical and Automation Engineering, The Chinese University of Hong Kong, Hong Kong, China. (email: (jmbstjtu@mae.cuhk.edu.hk, xychu@mae.cuhk.edu.hk, haozheng@cuhk.edu.hk, samuelau@cuhk.edu.hk) and [2]Department of Mechanical Engineering, The University of Hong Kong, Hong Kong, China (email: wangxmei@connect.hku.hk, kwokkw@hku.hk). *Corresponding Author: Jawad Mehmood Butt.

as SRT based aerial maneuvering, which was unavailable in the existing soft-tail research.

Although flight phase models with soft robotic tails were never investigated but several modeling strategies for different soft robots were proposed to understand their kinematic and dynamic motions [22], [23]. The kinematic models for soft robots were particularly illustrated with the assumption of Piecewise Constant Curvature (PCC) i.e., the transformation of infinite state space of the soft robots into the finite space, based on their motion characteristics [22]. Following the PCC assumption, some notable works such as finite element method (FEM) [24] and reduced-order model [25] were proposed for quasi-static applications but they usually required high gain feedback controllers and faced difficulties to generalize the highly dynamic motions. Besides, several finite-dimensional dynamic models such as discrete Cosserat model [26], Euler-Lagrange model [27], Kane's model [28], Ritz-Galerkin model [29], and other PCC based dynamic models [30], [31] were also proposed. These dynamic models were exemplary in their proposed context but rarely used in floating base soft robotic applications and seem analytically complex for the flight phase or angular momentum conservation modeling of the STAM system. To ensure the modeling simplicity of the STAM system, we target augmented rigid robot modeling approach [32], [33] because it uses conventional Denavit-Hartenberg (DH) formulation & PCC assumptions to model the soft robots, and will be an efficient solution to model the hybrid system (soft tail and rigid body). Hence, the objective of our work is to exploit the STAM system kinematics with PCC & ARR modeling methods [32], [33], and provide an analytically simple solution to the flight phase modeling and control of the STAM system.

In this work, the kinematics and flight phase model of 1-DOF STAM system are first derived by integrating the PCC & ARR modeling convention [32], which explains a systematic way to model the STAM systems. We then propose the soft tail arbitrary plane bending approach to extend the integrated modeling methods for the forward kinematics of the 2-DOF soft tail and STAM system. Together with the forward kinematics, the differential kinematics of 2-DOF STAM system are derived, i.e., the mapping of 2-DOF soft tail shape velocities with the body orientation angular rates and the actuation cable velocities respectively. These forward and differential kinematics are then utilized to derive the flight phase model of the 2-DOF STAM system. With the help of proposed kinematics and flight phase models, the flight phase control (kinematics based orientation control) is also proposed. This control is used to simulate the 1-DOF and 2-DOF STAM systems, which demonstrate the models effectiveness for the self-righting maneuvers.

The rest of the paper is structured as follows. The forward kinematics, differential kinematics and flight phase models for STAM systems are presented in Section II. Section III demonstrates the kinematics based orientation control and section IV illustrates the aerial self-righting simulation,

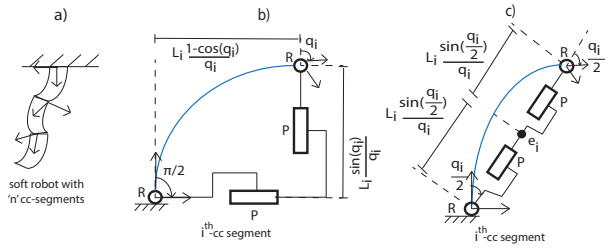

Fig. 2: Augmented Rigid Robot Structure to match the i^{th} segment of soft robot as a rigid robot. a) Soft robot with n cc-segments, b) RPPR structure to match the robot kinematics, b) RPPR structure to match the robot dynamics

which validates our proposed models and control. In the end, a discussion is carried out in section V which elaborates the empirical future of this work.

II. Modeling

This section presents the brief introduction to ARR modeling method and showcase the challenges & assumptions in STAM system modeling. The main aim is to formulate the 1-DOF and 2-DOF STAM system kinematics together with their flight phase models, which help our STAM systems in the conservation of the total angular momentum.

A. Brief Introduction to Augmented Rigid Robot Model

The kinematics of the soft robot are generally modeled by piecewise constant curvature (PCC) method where the shape of robot's multiple segment is modeled by multiple constant curvature (cc) arcs, which are then merged together such that the overall curvature is differentiable. The PCC method is also extended as the augmented rigid robot structure where the kinematics of the soft robot are modeled by matching its curvature by the combination of rigid revolute or prismatic joints [33].

Let us take a soft robot with n cc-segments as shown in Fig. 2a. A configuration variable q_i is defined to represent the bending angle of soft robot's i^{th} cc segment. Let us match the curvature of the i^{th} cc segment of soft robot with rigid Revolute-prismatic-prismatic-revolute (RPPR) structure as shown in Fig. 2b, where we define the rigid joint configuration variables for the i^{th} cc segment as $\varsigma_{rigid}(i) = (q_R, q_P, q_P, q_R)^T$. Let us include the inertial influence on the kinematic behavior of soft robot by matching the curvature and center of mass of each cc segment of the soft robot with the rigid RPPR structure and a point mass (Fig. 2c), which also treats the inertial properties of soft robot and augmented rigid structure equivalent [32]. The equivalent RPPR rigid robot structure to describe i^{th} cc segment is formulated by classical DH parametrization Table I, where a,d,θ,α are classical DH parameters, e_i is the segment point mass, and L_i is the length of cc segment. For i^{th} cc segment, the corresponding map from soft configuration to rigid configuration provided by ARR method is formulated in (1) respectively. (Read [32], [33] for details).

$$\varsigma_{rigid}(i) = \begin{bmatrix} \frac{q_i}{2} & L_i \frac{\sin(\frac{q_i}{2})}{q_i} & L_i \frac{\sin(\frac{q_i}{2})}{q_i} & \frac{q_i}{2} \end{bmatrix}. \quad (1)$$

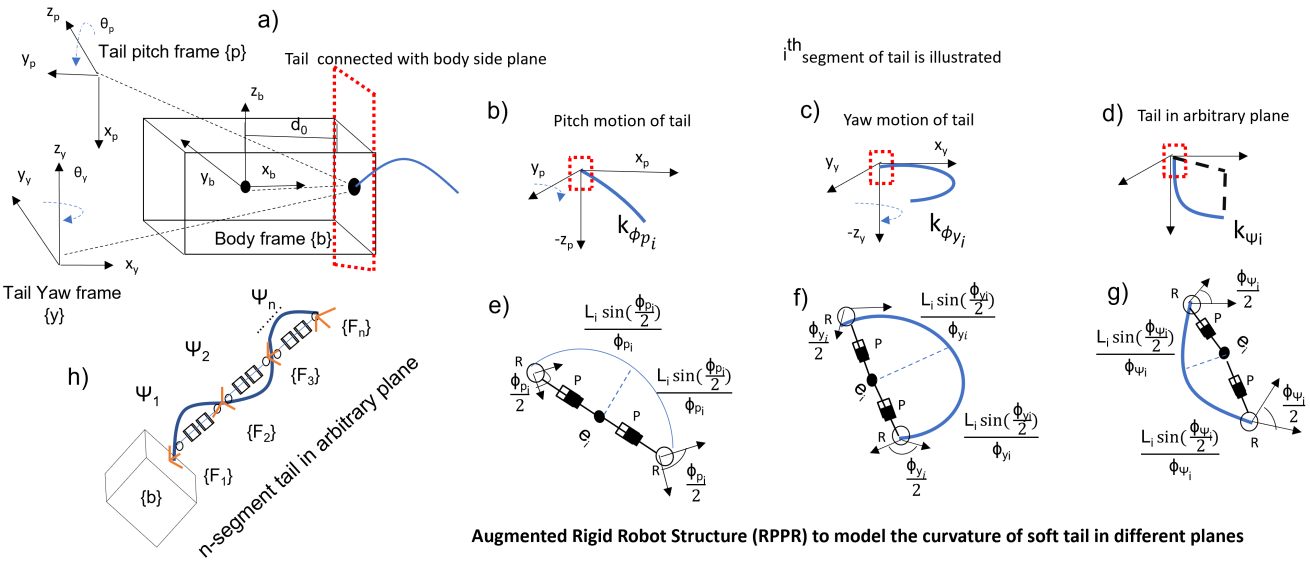

Fig. 3: a) Body frame assignment by DH convention, b-d) Tail motions in pitch, yaw, and arbitrary directions, e-g) Augmented rigid robot structures (RPPR) to model the curvature of soft tail in pitch, yaw, and arbitrary directions, h) n-segment soft tail attached with body. *Note that (b-g) represents i^{th} section of soft tail

TABLE I: Classical DH parametrization to describe i^{th} cc segment with RPPR rigid structure.

Link	θ	d	a	α	mass
1	$\frac{q_i}{2}$	0	0	$\pi/2$	0
2	0	$L_i \frac{\sin(\frac{q_i}{2})}{q_i}$	0	0	e_i
3	0	$L_i \frac{\sin(\frac{q_i}{2})}{q_i}$	0	$-\pi/2$	0
4	$\frac{q_i}{2}$	0	0	0	0

By using [34], the transformation matrix for i^{th} cc segment is written as $\boldsymbol{T}_i = \boldsymbol{T}_1^0 \boldsymbol{T}_2^1 \boldsymbol{T}_3^2 \boldsymbol{T}_4^3$, which can be extended to n-segment soft tail as $\boldsymbol{T}_n^0 = \boldsymbol{T}_i^0 ... \boldsymbol{T}_n^{n-1}$.

B. Challenges and Assumptions in STAM System Modeling

The modeling and control of the soft-tailed robots for the inertial-adjustment applications is a challenging task and it has been rarely studied in the past [16], [21]. In this section, we have discussed some challenges that are important to ponder before the explanation of our proposed work. First, mimicking animal-like robots for agile maneuvering applications is practically unrealistic due to their complex body structures. However, to achieve the natural imitation, the agile maneuvering robots can be simply treated as the robot with a rigid body (animal trunk), soft robotic tail (animal tail), and the actuation units (tail actuation joints) (Fig. 1). Second, to mimic the sweeping (pitch/yaw) and spiral (roll) motion of the animal tail, we need a compliant soft robot that can perform these maneuvers. In literature, we have only found the cylindrical soft-robots driven by 4-cables, which resembles the animal tail and can be used to perform these motions. Third, we have discovered that the twist motion of the assumed cylindrical soft robotic tail is not same like the roll motion of the animal tail [13] [21]. It is also not strong enough to adjust the body inertia in the roll direction because of cylindrical soft-tail structural symmetry. However, considering our work as a first step towards soft agile locomotion, we can use the 2-DOF's of the soft-tail (in-plane bending (pitch) and out-of-plane bending (yaw)) because they can satisfy the natural tail sweeping motions and are suitable for the body inertial-adjustment in the pitch and yaw directions.

C. 1-DOF STAM System Modeling

We consider a n-segment soft tail capable of bending in either pitch or yaw direction. The i^{th} segment of soft tail have the configuration variable ϕ_i (tail pitch - ϕ_{p_i} or yaw - ϕ_{y_i}) where its curvature is matched with a RPPR rigid joint structure. The joint variables of augmented rigid components are $\varsigma_i = [\varsigma_R, \varsigma_P, \varsigma_P, \varsigma_R]$, which are combined for n-cc-segments in vector form as $\boldsymbol{\varsigma} = [\{\varsigma_R, \varsigma_P, \varsigma_P, \varsigma_R\}_1, ..., \{\varsigma_R, \varsigma_P, \varsigma_P, \varsigma_R\}_n]^T \in \mathbb{R}^{4n}$.

For 1-DOF STAM system, the body is combined with the n-segment soft tail and the generalized coordinates are $\boldsymbol{\sigma} = [\theta, \boldsymbol{\varsigma}]^T$, where $\theta \in \mathbb{R}^1$ is either body pitch (θ_p) or yaw (θ_y) and $\boldsymbol{\sigma} \in \mathbb{R}^{4n+1}$ is a vector that contains body and augmented rigid joint states. Following (1), the non-linear constraints for soft tail i^{th} cc-segment which maps the soft tail state variable to the rigid tail joint states are shown in (2).

$$\varsigma_i = \begin{bmatrix} \frac{\phi_i}{2} & L_i \frac{\sin(\frac{\phi_i}{2})}{\phi_i} & L_i \frac{\sin(\frac{\phi_i}{2})}{\phi_i} & \frac{\phi_i}{2} \end{bmatrix}. \quad (2)$$

Let us consider the simple pitch case (Fig. 3b,e), where we use 1-segment soft tail ($n = 1$) attached to the rigid body. The generalized coordinates for pitch case are defined as $\boldsymbol{\sigma_p} = [\theta_p, \boldsymbol{\varsigma_p}]^T$, where $\boldsymbol{\sigma_p} \in \mathbb{R}^5$ and $\boldsymbol{\varsigma_p} \in \mathbb{R}^4$. (2) is used to map $\phi_p \in \mathbb{R}^1$ to $\boldsymbol{\varsigma_p}$. We reformulate the DH parameters for 1-DOF STAM system by using the DH parametrization as shown in Table II, where d_o is the tail offset from body center and L_1 is the length of 1-segment tail.

TABLE II: DH Parameters for 1-DOF STAM System.

Link	θ	d	a	α	mass
b	θ_p	d_o	0	0	0
1	$\frac{\phi_p}{2}$	0	0	$\pi/2$	0
2	0	$L_1\frac{\sin(\frac{\phi_p}{2})}{\phi_p}$	0	0	e_1
3	0	$L_1\frac{\sin(\frac{\phi_p}{2})}{\phi_p}$	0	$-\pi/2$	0
4	$\frac{\phi_p}{2}$	0	0	0	0

For flight phase model, we integrate the kinematic and inertial behavior of the 1-DOF STAM system for the conservation of total angular momentum. At kinematic level with inertia influence, we only need the inertia terms, body and tail velocities. By using Table II, we extract individual position information of the body and rigid tail components (p_R, p_p, p_p, p_R) from homogeneous transformation [34]. Then we calculate body inertia ($M_b \in \mathbb{R}^1$) in pitch direction from the solid cuboid moment of inertia formula and use $M_t = [M_R, M_P, M_P, M_R] = [\frac{e_1 p_R^2}{4}, \frac{e_1 p_P^2}{4}, \frac{e_1 p_P^2}{4}, \frac{e_1 p_R^2}{4}]$ for tail inertial terms, where we write $M = [M_b, M_t] \in \mathbb{R}^{1\times 5}$. Let us define the body angular momentum as H^b, and from the basic definition of angular momentum and [10], [12], we get

$$H^b = M\dot{\boldsymbol{\sigma}}_p \tag{3}$$

By assuming the zero angular momentum throughout the flight phase ($H^b = 0$), we rewrite the equation (3) for the flight phase model as,

$$0 = M_b\dot{\theta}_p + M_R\dot{\boldsymbol{\varsigma}}_R + M_P\dot{\boldsymbol{\varsigma}}_P + M_P\dot{\boldsymbol{\varsigma}}_P + M_R\dot{\boldsymbol{\varsigma}}_R, \tag{4}$$

$\dot{\theta}_p$ is body pitch velocity, and $\dot{\boldsymbol{\varsigma}}_R$, $\dot{\boldsymbol{\varsigma}}_P$, $\dot{\boldsymbol{\varsigma}}_P$, $\dot{\boldsymbol{\varsigma}}_R$ are the velocity of each joint belongs to RPPR structure. By substituting the derivatives of (2) we get $\dot{\boldsymbol{\varsigma}}_R$, $\dot{\boldsymbol{\varsigma}}_P$, $\dot{\boldsymbol{\varsigma}}_P$, $\dot{\boldsymbol{\varsigma}}_R$, and rewriting the flight phase model as,

$$0 = M_b\dot{\theta}_p + \frac{1}{2}\bar{M}_a + \bar{M}_b\dot{\phi}_p, \tag{5}$$

Rearranging (5) gives,

$$\dot{\phi}_p = -\bar{M_b}^{-1}(\ M_b\dot{\theta}_p + \frac{1}{2}\bar{M}_a)\ , \tag{6}$$

where $\bar{M}_b = (\ \frac{1}{2\phi_p}\cos\frac{\phi_p}{2} - \frac{1}{\phi_p^2}\sin\frac{\phi_p}{2})\ (\ 2M_P)$ and $\bar{M}_a = 2M_R$. The flight phase equation (6) will be further used for controller derivation in Section III-A

D. 2-DOF STAM System Modelling

1) Forward Kinematics of the Soft Tail

Let us consider a rigid body and soft tail consist of n-cc-segments and each is assigned with a reference frame $\{\boldsymbol{b}\}, \{\boldsymbol{F}_1\}, ... \{\boldsymbol{F}_n\}$ (Fig. 3h). The i^{th} segment of the soft tail has two configuration variables, i.e., in-plane bending (tail pitch - ϕ_{p_i}) and out-of-plane bending (tail yaw - ϕ_{y_i}). With mutual effect of pitch and yaw the soft tail is bending in an arbitrary plane which is referred as "Arbitrary plane bending". Here we present the arbitrary plane bending angle for the i^{th} segment as $\boldsymbol{\psi_i}$, where $\boldsymbol{\psi} \in \mathbb{R}^n$ is a set of all cc segments arbitrary bending configuration variables. The term $\boldsymbol{\psi_i}$ is proportionally related to the tail's curvature in arbitrary plane (k_{ψ_i}) that is defined as $\boldsymbol{\psi}_i = L_i k_{\psi_i}$ where L_i is the scalar length of i^{th} segment.

To derive the relation between $\boldsymbol{\psi}_i$ and 2-DOF tail (i^{th} section) bending angles ($\boldsymbol{\phi}_{y_i}, \boldsymbol{\phi}_{p_i}$), we relate the curvature of i^{th} segment as $k_{\psi_i} = \sqrt{k_{\phi_{p_i}}^2 + k_{\phi_{y_i}}^2}$ and get the desired bending relation as,

$$\boldsymbol{\psi}_i = \sqrt{\boldsymbol{\phi}_{p_i}^2 + \boldsymbol{\phi}_{y_i}^2}. \tag{7}$$

where $k_{\phi_{p_i}}$ and $k_{\phi_{y_i}}$ are the curvature variable in tail pitch and yaw directions (Fig. 3-b-d). The arbitrary plane bending angle is then used to formulate the DH parametrization of the 2-DOF soft tail by augmented rigid robot formulation (use Table I with ψ_i and see Fig. 3-e-g). The homogenous transformation of i^{th} cc segment is written as $\boldsymbol{T}_i = \boldsymbol{T}_1^0\boldsymbol{T}_2^1\boldsymbol{T}_3^2\boldsymbol{T}_4^3$ and for 2-DOF STAM system with n-segment tail, the transformations are accumulated as $\boldsymbol{T}_n^b = \boldsymbol{T}_i^b\boldsymbol{T}_{i+1}^i ... \boldsymbol{T}_n^{n-1}$ This helps us to explicitly control the arbitrary plane bending by inducing the simultaneous tail pitch and yaw input.

2) Body-Tail Kinematics

For 2-DOF STAM system, a rigid body is attached with n-segment soft tail (Fig. 3h). The rigid body has the yaw (θ_y) and pitch (θ_p) configuration variable ($\boldsymbol{\theta} = [\theta_y, \theta_p] \in \mathbb{R}^2$) and the soft tail has configuration variable $\boldsymbol{\phi} = [\phi_{y_1}, \phi_{p_1} ... \phi_{y_n}, \phi_{p_n}] \in \mathbb{R}^{2n}$. In this work, for simplification purpose we assume the rigid body is attached with a 1-segment soft tail where $\boldsymbol{\phi} = [\phi_y, \phi_p] \in \mathbb{R}^2$. The differential kinematics between the rigid body and soft tail are derived here to relate the body orientation angular rates with the tail shape velocities geometrically through a Jacobian matrix $\boldsymbol{J}_{\theta\phi}$ that reduces the coupling effect between the tail and body motions (in yaw and pitch directions).

Remark 1: The arbitrary plane bending with the reduced pitch and yaw coupling can be achieved by the explicit relation between the body and tail configuration variables. Explicit relationship (differential kinematics) is defined as the relationship of body pitch with tail pitch and relationship of body yaw with tail yaw.

Note that these geometrical relationships are derived only for the 1-segment soft tail but can easily be extended for the multi-segments soft tail. The geometric relation of ϕ_p with θ_p and ϕ_y with θ_y are shown in Fig. 4. We considered these geometrical relations as pure pitch and yaw relations and is derived as

$$a = \frac{\cos(\phi_p)L_1}{\phi_p}, b = \frac{\cos(\phi_y)L_1}{\phi_y}, \tag{8}$$

$$\theta_{p,\phi_p} = \sin^{-1}(\frac{d_o}{a}) \text{ and } \theta_{y,\phi_y} = \cos^{-1}(\frac{d_o}{b}), \tag{9}$$

where d_o is the distance between body center and tail origin, and L_1 is the length of the tail segment. The terms θ_{*,ϕ_*} defines the body state variables w.r.t to tail state variables. Without the loss of generality, it is practically assumed that body pitch or yaw is not disturbed by tail yaw or pitch respectively so $\theta_{p,\phi_y} = 0$ and $\theta_{y,\phi_p} = 0$. Taking the time derivative of θ_{*,ϕ_*} yields the Jacobian $\boldsymbol{J}_{\theta\phi} \in \mathbb{R}^{2\times 2}$ as,

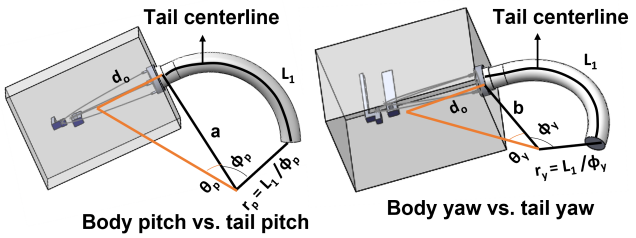

Fig. 4: Geometric description of the differential kinematics relating body orientation and tail shape parameters

$$\boldsymbol{J}_{\theta\phi} = \begin{bmatrix} 0 & \frac{\frac{d_0}{L_1 \cos(\phi_p)} + \frac{d_0 \sin(\phi_p)\,\phi_p}{L_1 \cos(\phi_p)^2}}{\sqrt{1 - \frac{{d_0}^2 {\phi_p}^2}{{L_1}^2 \cos(\phi_p)^2}}} \\ \frac{\frac{d_0}{L_1 \sin(\phi_y)} + \frac{d_0 \cos(\phi_y)\,\phi_y}{L_1 \sin(\phi_y)^2}}{\sqrt{1 - \frac{{d_0}^2 {\phi_y}^2}{{L_1}^2 \sin(\phi_y)^2}}} & 0 \end{bmatrix}, \tag{10}$$

where $\boldsymbol{J}_{\theta\phi}$ relates $\dot{\boldsymbol{\theta}} = \boldsymbol{J}_{\theta\phi}\dot{\boldsymbol{\phi}}$.

3) Cable-Tail Kinematics

The goal of this section is to calculate the Jacobian matrix $\boldsymbol{J}_{l\phi}$ that relates the approximate change in cable length with the tail shape velocities. We have assumed two pulleys connected with two different motors (for yaw and pitch motions) that wraps cables around its surface to produce linear cable displacement from motor rotation.

From the geometrical relationship between the pulleys, cables and the soft robot tail (see Fig. 5 - A general scenario where the change in pulley motion produces the change in cable length at the robot center-line). We can easily calculate the relation as $l_p = \frac{k_p + r_c}{\cos(\phi_p)}$ and $l_y = \frac{k_y + r_c}{\cos(\phi_y)}$, where l_p is the change in length of pitch cables (assumed at the soft center line), l_y is the change in the length of yaw cables (assumed at the soft center line), r_c is the radius of the pulley, k_p, k_y are soft tail curvature in pitch and yaw direction respectively. To move in the opposite direction we can use these relations with negative signs. Taking the time derivative we can get the desired Jacobian $\boldsymbol{J}_{l\phi} \in \mathbb{R}^{4\times 2}$ as

$$\boldsymbol{J}_{l\phi} = \begin{bmatrix} \boldsymbol{J}_1 & 0 & -\boldsymbol{J}_1 & 0 \\ 0 & \boldsymbol{J}_2 & 0 & -\boldsymbol{J}_2 \end{bmatrix}^T, \tag{11}$$

where $\boldsymbol{J}_1 = \frac{(\frac{\phi_y}{l_y} + r_c)\sin(\phi_y)}{\cos(\phi_y)^2}$ and $\boldsymbol{J}_2 = \frac{(\frac{\phi_p}{l_p} + r_c)\sin(\phi_p)}{\cos(\phi_p)^2}$. From Eq. 11 we can easily get rate of change in length in arbitrary plane as $\dot{\boldsymbol{l}} = \boldsymbol{J}_{l\phi}\dot{\boldsymbol{\phi}}$, where $\dot{\boldsymbol{l}} \in \mathbb{R}^4$.

4) Flight Phase Model

To induce the 2-DOF aerial maneuvering motion, we derive the angular momentum equation expressed in body frame ($\boldsymbol{H}^b$) as,

$$\boldsymbol{H}^b = \boldsymbol{I}^c \boldsymbol{w}^b + \bar{\boldsymbol{J}}_{\theta\phi}\dot{\bar{\boldsymbol{\phi}}}, \tag{12}$$

where $\bar{\boldsymbol{J}}_{\theta\phi} = \begin{bmatrix} \boldsymbol{J}_{\theta\phi}(1,1) & \boldsymbol{J}_{\theta\phi}(1,2) & 0 \\ \boldsymbol{J}_{\theta\phi}(2,1) & \boldsymbol{J}_{\theta\phi}(2,2) & 0 \\ 0 & 0 & 0 \end{bmatrix} \in \mathbb{R}^{3\times 3}$, $\dot{\bar{\phi}} = \begin{bmatrix} \dot{\phi}_y, \dot{\phi}_p, 0 \end{bmatrix}^T \in \mathbb{R}^{3\times 1}$ is the tail bending rates (no roll included), $\boldsymbol{w}^b = \begin{bmatrix} w_y, w_p, 0 \end{bmatrix}^T \in \mathbb{R}^{3\times 1}$ is the body angular velocity in body frame (identically zero roll velocity). The term $\boldsymbol{I}_c$ is formulated as,

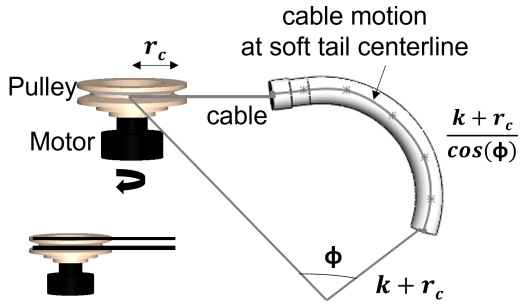

Fig. 5: Geometric visual description of the change in length of the soft robot by change in length of cable via pulley motion (General scenario applied to both pitch motion and yaw motion because we assume two individual pulleys for two different motions).

$$\boldsymbol{I}^c = \boldsymbol{I}^b - e_t(\hat{p}_t^b)(\hat{p}_t^b) \tag{13}$$

where $\boldsymbol{I}^b \in \mathbb{R}^{3\times 3}$ is the body moment of inertia, e_t is the tail mass, and $\hat{p}_t^b$ is skew symmetric matrix of position vector from tail to body.

The flight phase model is briefly described by (12), which explains that the total system angular momentum is the sum of joint space tail variables and the body angular momentum. Using the property of conservation of angular momentum altogether with the assumption of initial zero angular momentum and zero external disturbance, $\boldsymbol{H}^b$ will be zero during the flight phase. Based on this property and assumptions, we can get the angular velocity in the body frame as follows,

$$\boldsymbol{w}^b = -(\boldsymbol{I}^c)^{-1}\bar{\boldsymbol{J}}_{\theta\phi}\dot{\bar{\boldsymbol{\phi}}}. \tag{14}$$

III. Control Synthesis

The objective of this section is to apply the kinematics based orientation control to evaluate the effectiveness of the proposed models for the conservation of the total angular momentum. Here we derive the analytical control laws for 1-DOF and 2-DOF STAM systems that enforces tail cable velocities to extract required tail shape velocities for achieving the desired body orientation.

A. Kinematics Control for 1-DOF STAM System

To apply the kinematics based orientation control to the 1-DOF STAM system (to control the body pitch), we rewrite (6).

$$\dot{\phi}_p = -\bar{M_b}^{-1}(M_b\dot{\theta}_p + \frac{1}{2}\bar{M}_a)\ . \tag{15}$$

Eq. 15 describes the relation between the body pitch velocity and tail pitch velocity. As our actual input is the cable velocity, thus we need an explicit relation to relate the cable, tail and body. From the derived $\boldsymbol{J}_{l,\phi}$, $\boldsymbol{J}_{l,\phi}(2,2)$ and $\boldsymbol{J}_{l,\phi}(4,2)$ are the Jacobian entries that relates the tail pitch

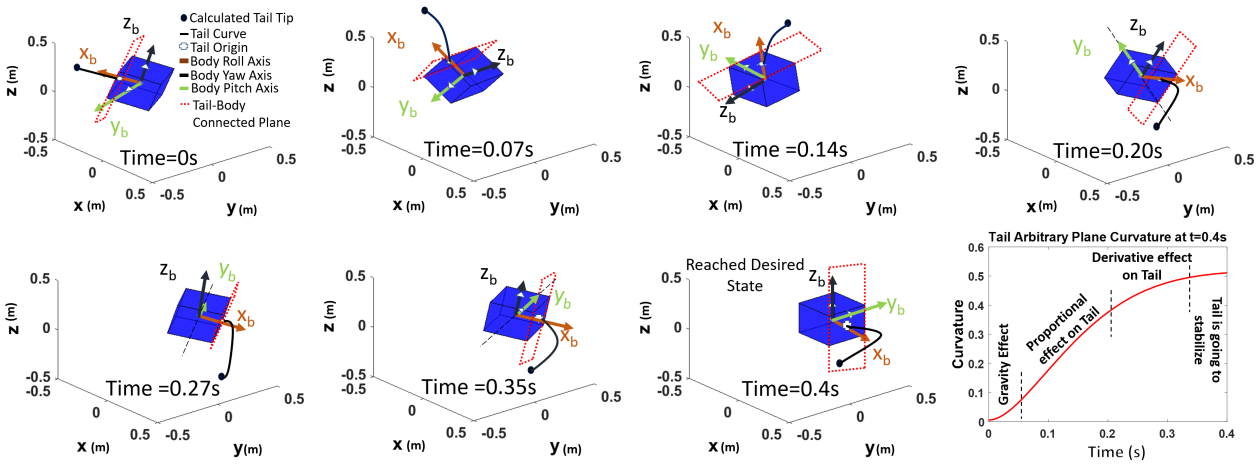

Fig. 6: Aerial self-righting animation scenario with 2-DOF flight phase control where body reached its desired states in 0.4s from initial states $[\phi_y, \phi_p] = [10^o, 8^o]$ by the motion inducing by soft tail. The first seven snaps shows the 2-DOF body orientation at t = 0s , 0.07s, 0.14s, 0.20s, 0.27s, 0.35s and 0.4s respectively. The last snap shows that how tail is responding from t = 0-4s and its different stages of control.

shape with the tail pitch cable velocity in the anticlockwise and clockwise pitch directions. Here we denote, $\boldsymbol{J}_{l,\phi}(*,2) = \boldsymbol{J}_{l,\phi}(2,2) = -\boldsymbol{J}_{l,\phi}(4,2)$ depending upon the direction of actuation. Substituting (15) in $\dot{l} = \boldsymbol{J}_{l,\phi}(*,2)\dot{\boldsymbol{\phi}}_p$ (here $\dot{l} \in \mathbb{R}^1$), we get the the final control relation that relates the body orientations and tail cable velocities as:

$$\dot{l} = -\boldsymbol{J}_{l\phi}(*,2)\bar{M_b}^{-1}(\ M_b\dot{\theta}_p + \frac{1}{2}\bar{M}_a)\ . \tag{16}$$

B. Kinematics Control for 2-DOF STAM System

We have also applied the kinematics control onto the 2-DOF STAM system to control the body orientation. To make the relation between the cable velocities, tail shape velocities and the body orientation, we will use two Jacobian relations $(\boldsymbol{J}_{\theta\phi}, \boldsymbol{J}_{l\phi})$ as described earlier. By using $\dot{\boldsymbol{\phi}} = \boldsymbol{J}^{+}_{l,\phi}\dot{l}$ and $\dot{\boldsymbol{\phi}} = \boldsymbol{J}^{-1}_{\theta\phi}\dot{\boldsymbol{\theta}}$ we get our proportional control equation as:

$$\dot{\boldsymbol{l}}_{prop} = g_p\boldsymbol{J}_{l\phi}\boldsymbol{J}^{-1}_{\theta\phi}(\boldsymbol{\theta}_{des} - \boldsymbol{\theta}), \tag{17}$$

where $\boldsymbol{\theta}_{des} \in \mathbb{R}^2$ is the desired body orientation and $g_p \in \mathbb{R}^{4\times4}$ is the diagonal proportional gain matrix. Looking at the $\boldsymbol{J}_{l,\phi} \in \mathbb{R}^{4\times2}$, the first two rows relates the cable direction with the soft tail shape velocities in one direction, while the last two rows keeps the direction in opposite direction. This confirms that, we can control the soft tail or indirectly the body orientation in anticlockwise and the clockwise direction. Thus, in our simulation, we keep track of our body initial conditions and use the Jacobian entries (either first two rows or last two rows denoted by $\boldsymbol{J}^{*}_{l\phi} \in \mathbb{R}^{2\times2}$, and the reduced order proportional gain matrix as $\bar{g}_p \in \mathbb{R}^{2\times2}$) to define the tail control direction. The reduced order controller equation is $\dot{\boldsymbol{l}}_{prop} = \bar{g}_p\boldsymbol{J}^{*}_{l\phi}\boldsymbol{J}^{-1}_{\theta\phi}(\boldsymbol{\theta}_{des} - \boldsymbol{\theta}) \in \mathbb{R}^2$. Also, we argue that the proportional control is not sufficient because it cannot overcome the effect of the tail velocities on the body, thus we have also applied the derivative control to reduce the effect of tail velocities on the body orientation as:

$$\dot{\boldsymbol{l}}_d = g_d(\dot{\boldsymbol{\phi}}_{des} - \dot{\boldsymbol{\phi}}), \tag{18}$$

where $g_d \in \mathbb{R}^{2\times2}$ is the diagonal derivative gain matrix and $\dot{\boldsymbol{\phi}}_{des} \in \mathbb{R}^2$ is the desired tail shape velocities. The overall kinematic control is $\dot{\boldsymbol{l}}_{kin} = \dot{\boldsymbol{l}}_{prop} + \dot{\boldsymbol{l}}_d \in \mathbb{R}^2$. The stability analysis of the PD type controller for fully actuated STAM system is not discussed here because it is similar to most of the stability analysis of fully actuated system found in [35].

IV. Simulation Results

Inspired by the self-righting characteristic of the animals through their tails, we have designed the simulation environment for 1-DOF and 2-DOF STAM systems with main simulation parameters (Table. III), which demonstrate the effectiveness of the soft-tail to control the body orientation in a free-fall scenario.

A. Simulation of 1-DOF STAM System

This section describes the simulation results of the planar orientation control of 1-DOF STAM system, where the tail pitch aids the body pitch to reach its desired position. In the simulation, we have made three cases where the initial body configuration of the body pitch was set as $34^o, 74^o$ and 120^o, and the desired body orientation was 0^o. The choice of initial conditions are random but are restricted to a maximum of 120^o because of natural flying cat imitation and low controller gain selection. The results in Fig. 7 shows the body can reach to the desired body orientation from different initial configurations with the aid of the tail movement.

B. Simulation of 2-DOF STAM System

The results are shown in Fig. 8 that illustrates the 2-DOF orientation control with the proposed approach. With the zero desired states and zero initial angular velocities, the initial body states (yaw, pitch) of $[10^o, 8^o]$ and $[20^o, 30^o]$ were provided. By tail action, the body reached its desired

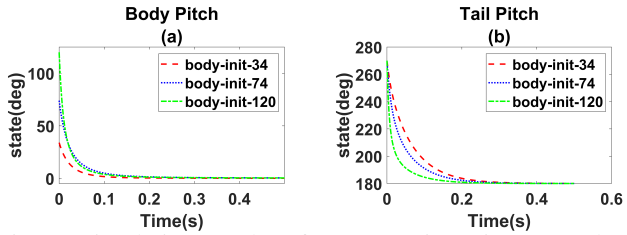

Fig. 7: Simulation results of 1-DOF orientation control: (a) Three graphical illustrations illustrate three different cases where the body is falling from three different pitch initial conditions, (b) the tail response for three different body falling cases respectively.

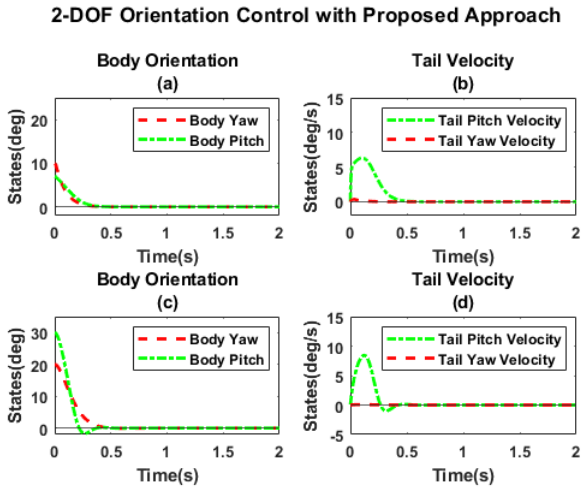

Fig. 8: Simulation results of 2-DOF orientation control: (a),(c) show that the body achieve the desired orientation from two different initial orientations, (b),(d) describe the tail velocities in two different orientation scenarios.

states in the span of $0.5s$ as shown in Fig. 8a and Fig. 8c respectively. Also, we argue that tail pitch velocity is always greater than its yaw velocity. This is due to the fact that in the arbitrary plane, yaw motion is the curvilinear deflection and it helps the tail to move out of the plane and then follows the leading curvature provided by the pitch motion. This argument is supported by Fig. 8b and 8d.

C. Aerial Self-Righting Animation Scenario

In the end, we show the animation snapshots in Fig. 6 that explains the 2-DOF orientation control of the body by the help of the soft tail. We here represent the body as a cuboid. Looking from the left, the body is at the initial conditions of $\boldsymbol{\theta} = [10^o, 8^o]$ and the tail possesses no curvature. Following the time, from $t = 0s$ to $t = 0.399s$, the tail is bending in the arbitrary plane and forced the body to change its orientation to the desired states. At last, mimicking the real-time scenario, the tail takes $0.40s$ to aid the body in achieving its desired states. It is important to note that one end of the tail is fixed with the body and the tail is bending in an arbitrary plane at an angle ψ. The last snapshot in Fig. 6 illustrates the arbitrary plane curvature (ψ) and we can easily observe the action of proportional and derivative control that helps to stabilize the tail in the end.

TABLE III: Simulation Parameters.

Parameters	Values	Units
Tail mass	0.2	kg
Body mass	0.8	kg
Tail length	0.4	m
Tail Offset from Body Origin	0.15	m
Body Moment of Inertia ($\boldsymbol{I}^b_{(xx,yy,zz)}$)	0.0075	kgm^2

V. Discussion

This paper provides the preliminary mathematical deduction of a model to accomplish soft-tail-based self-righting, and validates the orientation control performance via simulation. Aiming at transferring this virtual simulation outcome to an actual robotic system, we could notice that a key mechanical component is lacking, that is, a forceful soft actuator which can act as the artificial tail. An appropriate choice should enable fast-dynamic response and large-payload maneuvering, while an ordinary soft manipulator molding by elastic materials is far from qualification. A novel spring-reinforced actuator proposed in our previous work [36] is expected to take this tail-mimicking role.

Constructed by closed-coil spring backbone and silicone-bodied muscle, such an actuator is situated in the intermediate state of endoskeletal mechanisms and muscular hydrostats [36]. It enables a robust 0-to-90 bending in only $0.5s$, satisfying the rigorous response-speed requirement reflected in our simulation (Fig. 8), where the tail took around $0.5s$ for the body orientation control. Another notable advantage of the soft actuator comes from its approximately-linear omni-directional bending behavior, which significantly reduces the control or modeling burden of the actuator itself. It has also been tested via lifting and shifting a load, indicating its potential integration and coordination with a relative-heavy robot body. With the design of robotic tail determined, our future work will focus on implementing the modeling strategy to the real-time practical system. Experimental validations will also be conducted to promote our study in more generalized applications.

VI. Conclusion

This work proposed the kinematics modeling strategy to model the 1-DOF and 2-DOF soft-tail based aerial maneuvering (STAM) systems, derivation of flight phase models for the conservation of total angular momentum and the kinematics based orientation control. We have first integrated the PCC and ARR methods to model the forward kinematics of the 1-DOF STAM and derived its flight phase model. We then proposed the soft-tail arbitrary plane bending strategy to reformulate the ARR based DH parametrization for the forward kinematics of the 2-DOF soft tail. For 2-DOF STAM system, we derived the differential kinematics to map the tail shape velocities with the body orientation angular rates and the tail cable velocities respectively. By using these kinematic formulations we derived the flight phase model

for the 2-DOF STAM system, which is crucial for the conservation of the total angular momentum. In the end, we proposed the flight phase (kinematics based) orientation control, which is used to simulate the STAM systems for effective aerial self-righting maneuvers.

ACKNOWLEDGMENT

The authors would like to thanks Dr Xin Ma for their suggestions in improving the quality of the paper.

REFERENCES

[1] A. J. Ijspeert, "Biorobotics: Using robots to emulate and investigate agile locomotion," *science*, vol. 346, no. 6206, pp. 196–203, 2014.

[2] M. Rafeeq, S. F. Toha, S. Ahmad, and M. A. Razib, "Locomotion strategies for amphibious robots-a review," *IEEE Access*, vol. 9, pp. 26323–26342, 2021.

[3] A. Jusufi, D. I. Goldman, S. Revzen, and R. J. Full, "Active tails enhance arboreal acrobatics in geckos," *Proceedings of the National Academy of Sciences*, vol. 105, no. 11, pp. 4215–4219, 2008.

[4] E. Chang-Siu, T. Libby, M. Tomizuka, and R. J. Full, "A lizard-inspired active tail enables rapid maneuvers and dynamic stabilization in a terrestrial robot," in *2011 IEEE/RSJ International Conference on Intelligent Robots and Systems*, pp. 1887–1894, IEEE, 2011.

[5] A. M. Johnson, T. Libby, E. Chang-Siu, M. Tomizuka, R. J. Full, and D. E. Koditschek, "Tail assisted dynamic self righting," in *Adaptive Mobile Robotics*, pp. 611–620, World Scientific, 2012.

[6] J. Zhao, T. Zhao, N. Xi, M. W. Mutka, and L. Xiao, "Msu tailbot: Controlling aerial maneuver of a miniature-tailed jumping robot," *IEEE/ASME Transactions on Mechatronics*, vol. 20, no. 6, pp. 2903–2914, 2015.

[7] T. Libby, T. Y. Moore, E. Chang-Siu, D. Li, D. J. Cohen, A. Jusufi, and R. J. Full, "Tail-assisted pitch control in lizards, robots and dinosaurs," *Nature*, vol. 481, no. 7380, pp. 181–184, 2012.

[8] J. An, T. Chung, C. H. D. Lo, C. Ma, X. Chu, and K. S. Au, "Development of a bipedal hopping robot with morphable inertial tail for agile locomotion," in *2020 8th IEEE RAS/EMBS International Conference for Biomedical Robotics and Biomechatronics (BioRob)*, pp. 132–139, IEEE.

[9] D. De A, Koditschek, "The penn jerboa: a platform for exploring parallel composition of templates," *arXiv preprint arXiv:1502.05347*, 2015.

[10] E. Chang-Siu, T. Libby, M. Brown, R. J. Full, and M. Tomizuka, "A nonlinear feedback controller for aerial self-righting by a tailed robot," in *2013 IEEE International Conference on Robotics and Automation*, pp. 32–39, IEEE, 2013.

[11] G. Wenger, A. De, and D. E. Koditschek, "Frontal plane stabilization and hopping with a 2dof tail," in *2016 IEEE/RSJ International Conference on Intelligent Robots and Systems (IROS)*, pp. 567–573, IEEE, 2016.

[12] X. Chu, C. H. D. Lo, C. Ma, and K. W. S. Au, "Null-space-avoidance-based orientation control framework for underactuated, tail-inspired robotic systems in flight phase," *IEEE Robotics and Automation Letters*, vol. 4, no. 4, pp. 3916–3923, 2019.

[13] W. Saab, W. S. Rone, and P. Ben-Tzvi, "Robotic tails: a state-of-the-art review," *Robotica*, vol. 36, no. 9, pp. 1263–1277, 2018.

[14] A. D. Marchese, C. D. Onal, and D. Rus, "Autonomous soft robotic fish capable of escape maneuvers using fluidic elastomer actuators," *Soft robotics*, vol. 1, no. 1, pp. 75–87, 2014.

[15] J. L. C. Santiago, I. S. Godage, P. Gonthina, and I. D. Walker, "Soft robots and kangaroo tails: modulating compliance in continuum structures through mechanical layer jamming," *Soft Robotics*, vol. 3, no. 2, pp. 54–63, 2016.

[16] W. S. Rone *et al.*, "Maneuvering and stabilizing control of a quadrupedal robot using a serpentine robotic tail," in *2017 IEEE Conference on Control Technology and Applications (CCTA)*, pp. 1763–1768, IEEE, 2017.

[17] W. Saab, W. S. Rone, and P. Ben-Tzvi, "Discrete modular serpentine robotic tail: design, analysis and experimentation.," *Robotica*, vol. 36, no. 7, pp. 994–1018, 2018.

[18] W. Saab, W. S. Rone, A. Kumar, and P. Ben-Tzvi, "Design and integration of a novel spatial articulated robotic tail," *IEEE/ASME Transactions on Mechatronics*, vol. 24, no. 2, pp. 434–446, 2019.

[19] W. Rone, W. Saab, and P. Ben-Tzvi, "Design, modeling and optimization of the universal-spatial robotic tail," in *ASME International Mechanical Engineering Congress and Exposition*, vol. 58370, p. V04AT05A020, American Society of Mechanical Engineers, 2017.

[20] W. S. Rone, W. Saab, and P. Ben-Tzvi, "Design, modeling, and integration of a flexible universal spatial robotic tail," *Journal of Mechanisms and Robotics*, vol. 10, no. 4, 2018.

[21] Y. Liu and P. Ben-Tzvi, "Dynamic modeling, analysis, and comparative study of a quadruped with bio-inspired robotic tails," *Multibody System Dynamics*, vol. 51, no. 2, pp. 195–219, 2021.

[22] R. J. Webster III and B. A. Jones, "Design and kinematic modeling of constant curvature continuum robots: A review," *The International Journal of Robotics Research*, vol. 29, no. 13, pp. 1661–1683, 2010.

[23] D. Rus and M. T. Tolley, "Design, fabrication and control of soft robots," *Nature*, vol. 521, no. 7553, pp. 467–475, 2015.

[24] Z. Zhang, J. Dequidt, A. Kruszewski, F. Largilliere, and C. Duriez, "Kinematic modeling and observer based control of soft robot using real-time finite element method," in *2016 IEEE/RSJ International Conference on Intelligent Robots and Systems (IROS)*, pp. 5509–5514, IEEE, 2016.

[25] G. Runge and A. Raatz, "A framework for the automated design and modelling of soft robotic systems," *CIRP Annals*, vol. 66, no. 1, pp. 9–12, 2017.

[26] S. Grazioso, G. Di Gironimo, and B. Siciliano, "A geometrically exact model for soft continuum robots: The finite element deformation space formulation," *Soft robotics*, vol. 6, no. 6, pp. 790–811, 2019.

[27] V. Falkenhahn, T. Mahl, A. Hildebrandt, R. Neumann, and O. Sawodny, "Dynamic modeling of bellows-actuated continuum robots using the euler–lagrange formalism," *IEEE Transactions on Robotics*, vol. 31, no. 6, pp. 1483–1496, 2015.

[28] W. S. Rone and P. Ben-Tzvi, "Continuum robot dynamics utilizing the principle of virtual power," *IEEE Transactions on Robotics*, vol. 30, no. 1, pp. 275–287, 2013.

[29] S. H. Sadati, S. E. Naghibi, I. D. Walker, K. Althoefer, and T. Nanayakkara, "Control space reduction and real-time accurate modeling of continuum manipulators using ritz and ritz–galerkin methods," *IEEE Robotics and Automation Letters*, vol. 3, no. 1, pp. 328–335, 2017.

[30] A. D. Marchese, R. Tedrake, and D. Rus, "Dynamics and trajectory optimization for a soft spatial fluidic elastomer manipulator," *The International Journal of Robotics Research*, vol. 35, no. 8, pp. 1000–1019, 2016.

[31] V. Falkenhahn, A. Hildebrandt, R. Neumann, and O. Sawodny, "Model-based feedforward position control of constant curvature continuum robots using feedback linearization," in *2015 IEEE International Conference on Robotics and Automation (ICRA)*, pp. 762–767, IEEE, 2015.

[32] C. Della Santina, R. K. Katzschmann, A. Bicchi, and D. Rus, "Model-based dynamic feedback control of a planar soft robot: trajectory tracking and interaction with the environment," *The International Journal of Robotics Research*, vol. 39, no. 4, pp. 490–513, 2020.

[33] B. Jones and I. Walker, "Kinematics for multisection continuum robots," *IEEE Transactions on Robotics*, vol. 22, no. 1, pp. 43–55, 2006.

[34] J. J. Craig, *Introduction to robotics: mechanics and control, 3/E*. Pearson Education India, 2009.

[35] B. Siciliano, L. Sciavicco, L. Villani, and G. Oriolo, "Modelling, planning and control," *Advanced Textbooks in Control and Signal Processing. Springer,*, 2009.

[36] H.-C. Fu, J. D. Ho, K.-H. Lee, Y. C. Hu, S. K. Au, K.-J. Cho, K. Y. Sze, and K.-W. Kwok, "Interfacing soft and hard: a spring reinforced actuator," *Soft robotics*, vol. 7, no. 1, pp. 44–58, 2020.